Z. Phys. C – Particles and Fields 50, 91–101 (1991)

Zeitschrift für Physik C Particles and Fields

A numerical study of the small-x behavior of deep inelastic structure functions in QCD

J. Bartels[1], J. Blümlein[2], G.A. Schuler[1]*

[1] II. Institut für Theoretische Physik, Universität Hamburg, Luruper Chaussee 149, W-2000 Hamburg 50, Federal Republic of Germany
[2] Institut für Hochenergiephysik, Zeuthen, Platanenallee 6, O-1615 Zeuthen, Federal Republic of Germany

Received 3 September 1990

Abstract. A numerical study of the Gribov–Levin–Ryskin equation for deep inelastic structure functions in the small-x regions is performed. In the first part we study a simplified version which illustrates general features of the solution and also allows to investigate certain analytic properties. In the second part we formulate a more realistic version of the GLR equation and compute its solution, for different input distributions and for different values of the strength of the nonlinearity in the GLR equation. One of the conclusions is that, provided the input distribution is not too flat and the nonlinear coupling is not too small, deviations from the standard evolution may be visible at HERA.

1 Introduction

The small-x behaviour of deep inelastic structure functions in QCD represents one of the most interesting topics in investigating and testing QCD as the correct theory of strong interactions. Most likely, the small-x values at not too small values of Q^2 that will be accessible at HERA as well as at LHC or the SSC will mostly belong to the transition region that lies between the domains of perturbative QCD on the one side and the nonperturbative Regge limit on the other side. By the domain of perturbative QCD we mean the region of moderately small values of x (say, $x > 10^{-2}$ and $Q^2 > 10\,\mathrm{GeV}^2$), where the parton picture has been developed and applied successfully. Using well-established methods such as the operator expansion and the renormalization group equation, this region can be analyzed reliably and thus represents one of the cleanest QCD tests. Standard methods are the (linear) evolution equations, first derived and discussed by Gribov and Lipatov [1], Altarelli and Parisi [2] and Dokshitser [3]. In the limit of very small x, on the other hand, one expects to see new features inside the nucleon [4, 5]: the density of gluons and quarks becomes very high and a new dynamical effect of saturation is expected to stop the further growth of the structure functions. Ultimately, the physics in this region will be similar to that of the nonperturbative Regge limit which is still waiting for a satisfactory solution in QCD. However, the transition from the moderate-x region towards the small-x limit may very well be accessible to perturbation theory, and, hence, allows us to test the ideas about the onset of nonperturbative dynamics. This is what makes, from the theoretical point of view, the small-x behaviour of the QCD deep inelastic structure functions very interesting. From a more pragmatic point of view, it is clear that QCD investigations at future machines (HERA, LHC, SSC) will inevitably face the question how structure functions behave at very small values of x: a thorough theoretical understanding of this region will, therefore, be of extreme importance.

About ten years ago, Gribov et al. [4] have performed a detailed study within QCD of this region. They showed that the $x - Q^2$ plane has to be divided into three regions (in what follows we will always assume Q^2 to be larger than a few GeV^2): at x of the order unity the standard evolution equations [1–3] are valid. They are based upon the sum of QCD-ladder diagrams. At smaller values of x non-ladder contributions become important and have to be added. Gribov, Levin and Ryskin were able to isolate the leading contributions: the multi-ladder diagrams (so-called fan-diagrams). Beyond this transition region many more Feynman diagrams and, eventually, also nonperturbative contributions have to be taken into account, leaving the Regge limit a still open problem. The transition region extends the region of applicability of perturbative QCD towards smaller values of x. The sum of the fan diagrams which forms the basis for the QCD description in this region can also be viewed as "screening" or "absorbtive corrections". Making certain assumptions about the coupling of these multiladder diagrams to the partons inside the nucleon, the sum of these diagrams has been shown to satisfy a nonlinear integro-differential equation (henceforth referred to as GLR-equation). The analysis of this equation appears to be highly nontrivial: apart from a few qualitative properties that have been

* Supported by Bundesministerium für Forschung und Technologie, 05 4HH 92P/3, Bonn, FRG

discussed already in [4], no systematic investigation has been done. In particular, methods that allow a careful numerical analysis will have to be developed and tested; once such a method has been found, the most urgent question concerns the precise location of the transition region: how far in x, Q^2 can we use standard perturbation theory [1–3], where should one use the improved description [4] of the fan-diagrams, and where should we expect to face the breakdown of perturbation theory? A first attempt to answer some of these question has recently been made by Collins and Kwiecinski [6].

In this paper we discuss numerical solutions of the GLR equation. As a start, we consider a somewhat simplified version of this equation keeping only the leading terms both in $\ln\frac{1}{x}$ and in Q^2. It allows to discuss some analytic properties explicitly, but its solution has only qualitative character. This "toy model" illustrates one of the important features of the GLR equation: the equation predicts its limit of applicability. To be more quantitative we then solve numerically a more realistic version of the GLR equation: the result, depending upon the input distribution and the strength of the nonlinearity in the GLR equation, indicates where in the $x - Q^2$ plane the GLR equation should be used instead of the usual linear evolution equation.

The main results of our analysis are described as follows. The nonlinear term in the GLR equation results in a much weaker rise at small x-values, compared to the standard linear evolution. In fact, at very small x-values the structure function becomes flat, thus confirming the idea of saturation of slow partons. It should, however, be kept in mind that the region of validity of the GLR equations ends before saturation is reached. As it had been already indicated in [4], a promising method of analyzing the GLR equation is the semi-classical approximation. In this picture one follows the evolution of the structure function along classical paths in the $x - Q^2$ plane. In case of the linear evolution equation which is valid for moderately small values of x these paths are straight lines ("rays"). In contrast, the GLR equations lead to slightly curved rays which are reflected along a boundary line (also called "critical line"). This line plays a fundamental role; in particular, it determines the location of the transition region in the $x - Q^2$ plane. An interesting feature of the GLR equation is also the fact that the input distribution at some small Q_0^2 is required only for $x < x_0$ where x_0 is the value of the boundary line at $Q^2 = Q_0^2$. This information seems to be sufficient to predict, for higher Q^2, the x-distribution at smaller values of x. We illustrate this for the case of the "toy model", but more theoretical work needs to be done before a similar analysis can be carried out also for the full GLR equation.

The numerical results that we present depend on the choice of the (nonperturbative) initial x-distribution at Q_0^2, as it does also in the case of the standard evolution. Further, the results depend upon the strength of the nonlinearity in the GLR equation, i.e. the value of the triple ladder vertex and the coupling of the first two-ladder diagrams to the hadron, relative to the one-ladder diagrams. These degrees of freedom are not predicted by perturbation theory but have to be determined by fitting the open parameters to experimental data. In this paper we choose one of the current parametrizations of the input densities and vary the two-to-one-ladder strength factor in some range. Then our results indicate that the nonlinear effects of the GLR equation may set in as early as at $x = 10^{-2}$ (for $Q^2 = 10\,\mathrm{GeV}^2$), and hence could be visible at HERA and at the Tevatron through the analysis of the low mass dimuon events at CDF and D0 in the very forward direction. With these forthcoming data and more theoretical and numerical work along the line of this paper the interesting question of the transition region should be settled soon.

The organization of this paper is the following. We first describe the different versions of the GLR equation that we are going to study. In Sect. 3 we present numerical results of the simplest approximation. Section 4 contains the analytic investigation in the framework of the semi-classical approximation. In Sect. 5 we describe a more realistic version of the GLR equation and present its numerical results. We then summarize and discuss our results in a final concluding section.

2 The Gribov–Levin–Ryskin equation

The equation that has been proposed by Gribov et al. [4] is illustrated in terms of Feynman diagrams in Fig. 1. It represents the sum of the so-called fan diagrams, where each single ladder denotes the standard Altarelli–Parisi evolution for gluons. Fermionic degrees of freedom are small compared to the gluon at small-x and are neglected in [4]. The GLR equation is formulated for $\phi = \frac{\partial F}{\partial Q^2}$ with $F = xG(x, Q^2)$ the gluon momentum density, and it has

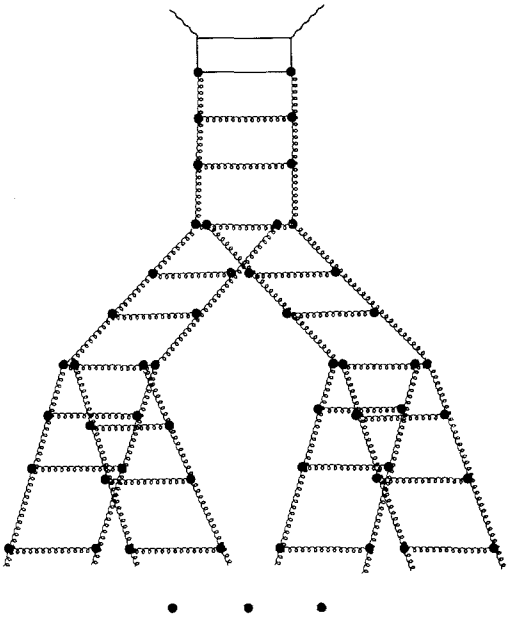

Fig. 1. Fan diagrams which are the basis for the GLR equation. The wavy lines denote gluons

the following form:

$$\frac{\partial\phi(x,q^2)}{\partial\ln\left(\frac{1}{x}\right)}=\int\tilde{K}(q^2,q'^2)\phi(x,q'^2)\frac{4N\alpha_s(q'^2)}{4\pi}dq'^2$$
$$-\frac{1}{4\pi R^2}\left(\frac{\alpha_s(q^2)}{4\pi}\right)^2 V\phi^2(x,q^2). \tag{2.1}$$

Here we have adopted the notation of [4]: x and Q^2 are the standard variables used in the Bjorken limit; in addition to these we use

$$\xi=\ln\ln\frac{Q^2}{\Lambda^2},\quad y=\frac{8N_c}{\beta_0}\ln\left(\frac{1}{x}\right)\quad\text{with}\quad\beta_0=\tfrac{11}{3}N_c-\tfrac{2}{3}n_f.$$

Numerically, $y\approx 6.6\cdot\log_{10}\left(\frac{1}{x}\right)$ for $n_f=4$, and $\xi\approx 1.502$ (2.683) for $Q^2=4\,\mathrm{GeV}^2$ ($10^5\,\mathrm{GeV}^2$). The QCD scale parameter Λ will be taken to be 0.212 GeV and the one-loop formula for the strong coupling constant is being used, $\alpha_s(Q^2)=4\pi/(\beta_0\ln(Q^2/\Lambda^2))$. In (2.1) the first term is linear in ϕ and contains the usual splitting function, where the gluonic part has been corrected to include the kernel of the Lipatov equation [7]. The second term, nonlinear in ϕ, describes the recombination of two ladders into one. The expression V for the triple ladder vertex is obtained by a saddle point approximation of the Feynman diagrams Fig. 1. The parameter R denotes the size of the nucleon and is related to a scale Q_0^2 above which $\alpha_s(Q^2)$ is small enough so that perturbative QCD can be applied. It follows from this equation that the coupling of two ladders at the bottom (Fig. 1) is not independent from that of one ladder: by iteration of the equation one finds that the probability of finding inside the nucleon two gluons with momentum fractions x_1, x_2 has been assumed to be proportional to the square of the corresponding one-gluon distribution. It is important to note that this equation describes the evolution in y and not in $\ln Q^2$, in contrast to the usual Altarelli–Parisi equation. Consequently, initial conditions are not prescribed at fixed Q_0^2 as a function of x (or y) but at fixed x as a function of Q^2. This indicates that the evolution scenario will be quite different from that in [1–3].

As a preparatory exercise, Gribov, Levin, and Ryskin suggested to study, instead of (2.1), a somewhat simpler version:

$$F(y,\xi)=F_G(y,\xi)-\int_0^y dy'\int_{\xi_0}^{\xi}d\xi' F_0(y-y',\xi-\xi')$$
$$\cdot C\exp(-e^{\xi'}-\xi')F^2(y',\xi').$$
$$F_G(y,\xi)=G(y)+\frac{1}{2}\int_0^y dy'\int_{\xi_0}^{\xi}d\xi' F_G(y',\xi')$$
$$F_0(y,\xi)=1+\frac{1}{2}\int_0^y dy'\int_0^{\xi}d\xi' F_0(y',\xi'). \tag{2.2}$$

Apart from the form of the triple-ladder vertex which now appears under the momentum integral, this equation can be derived from (2.1) by simply approximating the gluon splitting function by its most singular (for $x\to 0$) contribution, $P_{gg}(z)\to 6/z$, and by rewriting (2.1) in the form of an integral equation. $F_G(y,\xi)$ and $F_0(y,\xi)$ denote the sum of (gluonic) QCD ladder graphs with the initial condition $F_G(y,\xi_0)=G(y)$, $F_G(0,\xi)=0$ and $F_0(y,0)=F_0(0,\xi)=1$, respectively. In the original paper [4] (2.2) was discussed only up to constants. Correspondingly the authors of [4] set $\xi_0=0$ and used $F_G(y,\xi)=F_0(y,\xi)$. The quantity C was simply taken to be $C=1$. With these boundary conditions the solution of the linear equation for $F_G(y,\xi)$ is just the Bessel function $I_0(z)$ where $z=\sqrt{2y\xi}$.

An improved treatment of (2.2) requires, in particular, a more realistic choice of initial conditions. In a first step, one might follow the same strategy which is used for the linear evolution equation, i.e. specify F along the y-axis at a fixed Q_0^2. In (2.2) this is achieved by taking $F_G(y,\xi)$ again to be the sum of the gluonic ladder diagrams but with $F_G(y,\xi_0)=G(y)$, where $G(y)$ is the x-distribution at $Q^2=Q_0^2$. In general, the distribution along the ξ-axis is then determined through (2.2). Furthermore the quantity C has to be calculated. It consists of two factors, the relative strength of the two-gluon $G_{(2)}$ to the (usual) single-gluon distribution function G, and the triple ladder vertex coupling G_{3P}. The former term cannot be calculated from perturbative QCD but has to be taken as input. Following [8] we assume $G_{(2)}=Q_0^2/(4\pi)G(y)^2$. The triple ladder vertex coupling G_{3P} is calculated from all triple ladder diagrams yielding $G_{3P}=\pi^2\alpha_s(Q^2)/(C_F Q^2)$. This gives

$$C=\frac{3\pi^2}{4\beta_0}\frac{Q_0^2}{\Lambda^2}. \tag{2.3}$$

Note that

$$C\exp(-e^{\xi}-\xi)=\frac{3\pi}{16}\alpha_s(Q^2)\frac{Q_0^2}{Q^2}, \tag{2.4}$$

showing that the fan diagrams are higher twist contributions.

It should, however, be emphasized that this way of choosing initial conditions is not the only possibility. In fact, as we have said before, the first version of the GLR-equation (2.1) is an evolution equation in y, and it thus seems more natural to specify the initial conditions at fixed y rather than at fixed Q^2. If, on the other hand, this is done at a small value of y where the nonlinear term can safely be disregarded, then this (fixed-y, Q^2) distribution must be connected, through the usual linear evolution equations, with some (fixed-Q^2, y) distribution. The two ways of specifying initial conditions should therefore be equivalent, and it becomes a matter of practical convenience which one to choose. In our calculations, we adopt the "conventional" method.

It is convenient to rewrite (2.2) as an equation for F, eliminating both F_0 and F_G. The result is

$$F(y,\xi)=G(y)+\int_0^y dy'\int_{\xi_0}^{\xi}d\xi' F(y',\xi')$$
$$\cdot(\tfrac{1}{2}-C\exp(-e^{\xi'}-\xi')F(y',\xi')). \tag{2.5}$$

Equivalently, one could use differential equations for either $\frac{\partial F}{\partial y}$ or $\frac{\partial F}{\partial\xi}$ or $\frac{\partial^2 F}{\partial y\partial\xi}$ (each with the according

boundary conditions), e.g.

$$\frac{\partial^2 F(y,\xi)}{\partial y \partial \xi} = \frac{1}{2} F(y,\xi)(1 - 2C\exp(-e^{\xi} - \xi) F(y,\xi)) \qquad (2.6)$$

and

$$\frac{\partial F(y,\xi)}{\partial \xi} = \int_0^y dy' F(y',\xi)[\tfrac{1}{2} - Ce^{-e^{\xi}-\xi} F(y',\xi)]. \qquad (2.7)$$

Since the linear term of this approximation to the GLR equation sums the leading powers of both $\log Q^2$ and $\log\frac{1}{x}$, it has been named double-leading-log-approximation, DLA. Note, however, that this name only refers to the ladders inside the fan diagramas; the fan diagrams on the whole are of higher order in $1/Q^2$. It is the form (2.5) of the GLR equation that we will investigate first. We will denote it as "DLA + fan" approximation.

3 The numerical solution of the GLR equation (2.5)

The GLR equation (2.5) is a nonlinear integral equation of the Volterra-type in both variables. The solution $F(y,\xi)$ is bounded from above by the solution $F_0(y,\xi)$ of the linear problem ($C = 0$). Choosing $G(y)$ as a continuously differentiable function for all y the existence and uniqueness of the solution of (2.5) can be shown [9] for $F(y,\xi) \geqq 0$.

Due to this proof, the equation can be solved by discretizing the integral (2.5) in y and ξ. We have applied three different methods: (i) the solution of the discretized integral equation was determined by stepwise evolution solving one quadratic equation at each step; (ii) differentiating (2.5) with respect to y, we obtain the integro-differential equation (2.7) which has been solved numerically; (iii) we have integrated (2.6) with the boundary conditions $F(y,\xi_0) = G(y)$ and $F(0,\xi) = 0$.

For the initial distribution we choose

$$F(y,\xi_0) = G(y) = (1-x)^5 \exp\sqrt{cy} \qquad (3.1)$$

at $Q_0^2 = 4\,\mathrm{GeV}^2$ ($\xi_0 = 1.52$). The exponential factor in (3.1) was introduced to account for the asymptotic behaviour of the linear solution at small x. We choose $c = 6 \times 10^{-4}$ which yields a modification of the term $(1-x)^5$ by less than 10% for $x > 10^{-2}$. We checked that the numerical results obtained by the three different methods described above agree on the per cent level.

In Fig. 2a and b the solution of (2.5) is given as a function of y at different values of Q^2. For comparison the corresponding curves obtained for linear evolution are also shown. These show the well known exponential growth at large y. The main effect of the nonlinear term is a substantial flattening towards large y (i.e. small x). For comparison we also show the correction due to the first fan diagram. For moderate values of y it provides a rather reliable estimate of the effect of the nonlinear term. In Fig. 3a and b we have extended the y-axis up to exceedingly large y-values: the curves reach saturation. For smaller values of Q^2 (Fig. 3a) the curves oscillate before they reach the final plateau, for larger values of Q^2

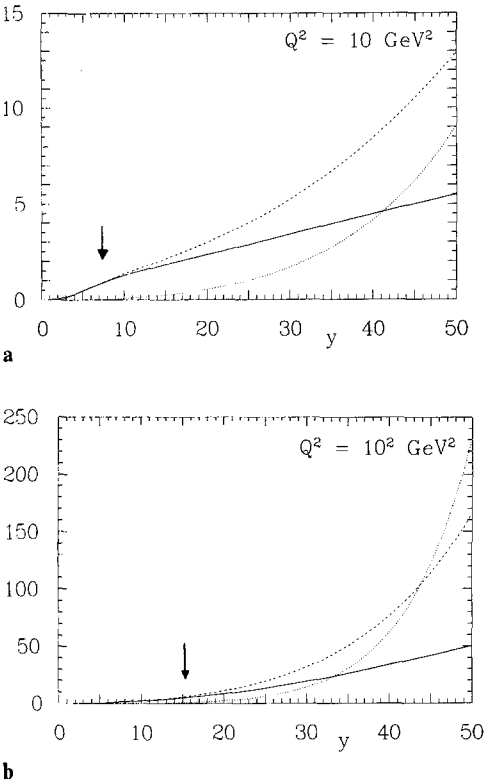

Fig. 2a, b. Distributions of F in y at two different values of Q^2 for the "DLA + fan" approximation (2.5) of the GLR equation. The dashed curves belong to the linear evolution ($C = 0$), the full ones to the full nonlinear equation. The dotted curves show the first fan diagram only. The arrows mark the critical line

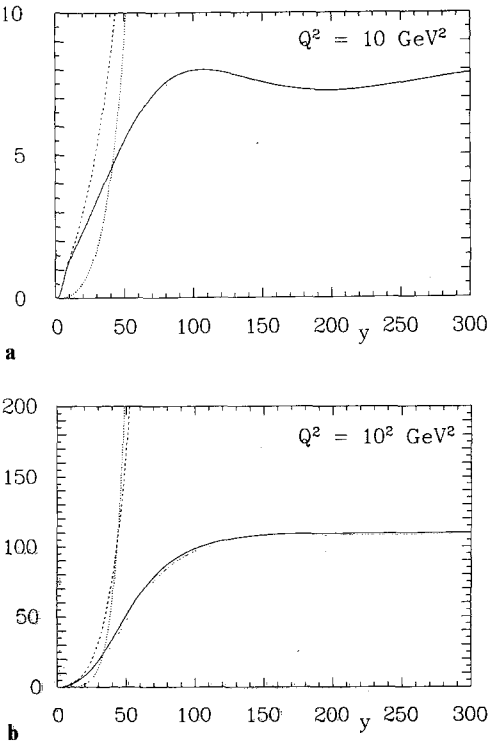

Fig. 3a, b. Same as Figs. 2a and b but with different scales in y

these oscillations persist but become small compared to the height of the plateau and thus are no longer visible.

The effect of saturation is quite in agreement with model calculations by A. Mueller [10], and it can be derived from (2.5) also by direct calculation [6]: at fixed ξ, the asymptotic ($y \to \infty$) solution of (2.5) is given by $F(y,\xi) \to 1/(2C)\exp(e^{\xi}+\xi)$. However, as we will discuss below, the plateau is already outside the region of validity of (2.5). We finally mention that for larger values of Q^2 the characteristics of Figs. 2a–3b do not change: the plateau grows higher, and it shifts towards larger values of y.

4 The semiclassical approximation

We now turn to an attempt to understand the situation in a more analytic manner. In [4] it had already been suggested that (2.6), for large values of ξ and y, could be investigated in terms of a semi-classical approximation. With the ansatz $F = \exp(S)$, the partial differential equation (2.6) of second order for F turns into a partial differential equation of first order for S:

$$S_y S_\xi = \tfrac{1}{2} - C\exp(S - e^{\xi} - \xi) \tag{4.1}$$

with $S_a \equiv \partial S/\partial a$. This equation is valid as long as the following condition is satisfied:

$$S_y S_\xi \gg S_{y\xi}. \tag{4.2}$$

Equation (4.2) can be solved with the methods of characteristics. This leads to the following set of ordinary differential equations ("evolution equations"):

$$\begin{aligned}
\dot{y} &= S_\xi \\
\dot{\xi} &= S_y \\
\dot{S} &= 2S_y S_\xi \\
\dot{S}_y &= -C\exp(S - e^{\xi} - \xi) S_y \\
\dot{S}_\xi &= -C\exp(S - e^{\xi} - \xi)(S_\xi - 1 - e^{\xi}).
\end{aligned} \tag{4.3}$$

Here the derivative symbol $\dot{y}$ etc. refers to the "inner" time along trajectories in the (ξ, y)-plane. It is straightforward to eliminate this time variable and to reduce the set of five equations to another set of four. A first numerical inspection of the validity condition (4.2) shows that it is satisfied for sufficiently large S. This excludes the regions close to the ξ axis (i.e. y near zero or x near 1) and, depending upon the initial y-distribution chosen at Q_0^2, possibly also the region of low Q^2. In particular, one has to be careful in applying this method in the most straightforward way: choose some initial y-distribution at Q_0^2 and use (4.3) to evolve towards larger Q^2. Moreover, the condition (4.2) is also not fulfilled near the plateau where both S_y and $S_{y\xi}$ are small. In order to make correct use of this semi-classical approximation we therefore adopt the following strategy. We select a region in the (y,ξ) plane where both y and ξ are reasonable large and where the condition (4.2) is satisfied. As starting values for the evolution equations (4.3), we then use those values for

$$S = \ln F, \quad S_y = \frac{F_y}{F}, \quad S_\xi = \frac{F_\xi}{F}$$

which we have calculated numerically in the previous section and evolve backwards, i.e. towards lower values of y and ξ.

The results of this calculation, for a whole set of such trajectories in the (y,ξ)-plane, are shown in Fig. 4, both for the linear case (Fig. 4a) and for the GLR equation (Fig. 4b). In the former case, the trajectories are straight lines ("rays") which, starting from the lower left corner, cover the whole (y,ξ)-plane in such a way that each point can be reached by exactly one ray (this also holds for the y-axis, although the density of trajectories seems to increase towards larger y-values). As soon as the nonlinear term in the GLR equation is turned on this picture changes quite essentially: the (y,ξ)-plane appears to be divided into two distinct regions. If we concentrate on trajectories which, at some reasonably large Q^2 value, start at a not too large y-value, and follow this trajectories

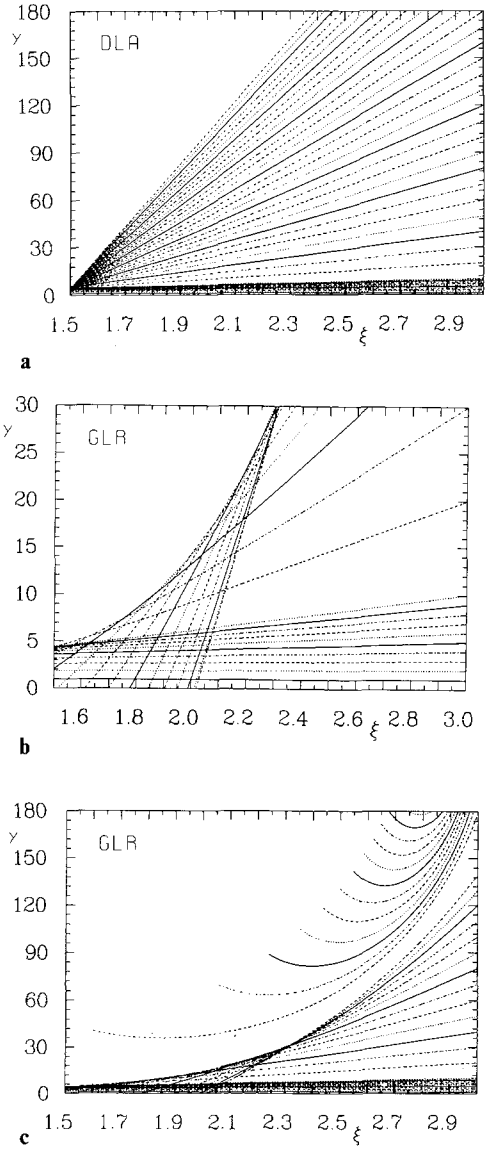

Fig. 4a–c. Pattern of trajectories in the "DLA + fan" approximation. **a** linear case, **b** nonlinear case, **c** a few trajectories in the "non- perturbative" region

backwards, i.e. towards the origin, then these trajectories seem to stay away from a region in the upper left corner. Moreover, each trajectory undergoes a slight bending as soon as it comes close to the boundary line between the "empty" and the "full' area. The boundary line between the two regions is the envelope to the trajectories which cover the "full" region. In the latter part of the (y, ξ)-plane there is another new feature, compared to the linear case of Fig. 4a: each point (excluding those on the boundary line) appears to be an intersection point of two different trajectories. Finally, far away from the boundary line the trajectories are again straight lines, just as in the linear case: the influence of the nonlinear term, therefore, is only felt at those points in the (y, ξ)-plane, for which the trajectories leading to this point have come close to the boundary line (below we shall argue that it should be only the flatter of the two trajectories to which this argument applies). This includes, approximately, all points above that line in Fig. 4b which is tangent to the boundary line on the y-axis. So far our discussion has been restricted to those trajectories which do not start at large values of y. If we now choose, as a starting point for our backward evolution, a point at very large y, i.e. inside the (so far) empty region, then this trajectory shows a quite different behaviour (examples are shown in Fig. 4c). It stays above the boundary line and, at smaller values of ξ, it eventually moves upwards. As a result, there seems to be a separation of the two regions. It is clear that the quantitative details of this whole picture will depend upon the initial y-distribution along the y-axis. The general form, however, is the same for a rather large variety of initial distributions.

Before we try to analyze this situation in further detail, we remind that these findings are quite in agreement with what has been discussed already in [4]. In the context of the GLR-equation (2.2) it has been shown that in addition to the trajectories (there named "group trajectories") there exists a distinguished path which is both "group and phase trajectory". This is exactly the boundary line in Fig. 4, and, for large ξ, it has the form

$$y_c(\xi) = \tfrac{1}{4}\exp 2\xi. \tag{4.4}$$

Along this line, S behaves as:

$$S(\xi) = \exp \xi - \ln C. \tag{4.5}$$

We emphasize, however, that both results are valid only asymptotically, and for finite ξ there are other, nonleading terms on the right hand side, e.g. in (4.4) a constant piece. The latter one cannot be computed analytically from the semi-classical approximation of the GLR equation alone but depends on the initial conditions on the y-axis. Our numerical analysis, in fact, shows that the asymptotic form (4.4) is not a very good approximation for realistic values of ξ.

In order to get a better understanding of Fig. 4b, we make use of the fact that (2.6) is, in fact, a two-dimensional wave equation, and the influence of the nonlinear term in (2.6) is quite analogous to a space-time dependent refraction index in an optical medium. In this language, our trajectories are light rays, and the boundary line in Fig. 4b is a line of focal points (i.e. a caustic), where the light rays are reflected. This type of a caustic can be handled by standard methods. A classification of caustics in terms of singularities of mappings can be found in [11]. Within this classification, our caustic is of the simplest type, a fold. In the vicinity of such a caustic, the form of the semi-classical (or eikonal) amplitude is universal, i.e. it only depends upon the type of the caustic. The general idea of constructing such an amplitude is described, e.g., in [12]. For illustration, we outline the construction of an amplitude F which, on the critical line (4.4), has the behaviour (4.5) and, a little below the line, reproduces the pattern of trajectories as shown in Fig. 4b.

First switch from the coordinates ξ, y to another set of variables in which the line (4.4) coincides with one of the axis ($y \equiv 0$). A simple choice is:

$$\begin{aligned} \xi' &= (y + \tfrac{1}{4}\exp 2\xi)^{1/4} \\ y' &= y - \tfrac{1}{4}\exp 2\xi. \end{aligned} \tag{4.6}$$

In these variables the following form of F fulfills all our requirements:

$$F(y', \xi') = \text{const.} \int \frac{dp'\,dq'}{2\pi i} \exp\left\{ -ip'\xi' + q'y' + \frac{1}{4\sqrt{2}} p'^2 + \tfrac{1}{3}q'^3 \right\}. \tag{4.7}$$

Here the integrations are along the imaginary axis: the p'-integral is gaussian, and the q'-integral is an Airy-integral. For large y' and ξ' the integral can be evaluated with the help of the saddle point approximation. For each point below the ξ'-axis (we restrict ourselves to $\xi' > 0$) there are two solutions:

$$p' = i2\sqrt{2}\xi', \quad q' = \pm\sqrt{-y'} \tag{4.8}$$

with

$$\begin{aligned} F = \frac{\text{const.}}{\sqrt[4]{-y'}} &\left(\exp\left\{\sqrt{2}\xi'^2 + \tfrac{2}{3}\sqrt{(-y')^{3/2}}\right\}\right. \\ &\left. - \exp\left\{\sqrt{2}\xi'^2 - \tfrac{2}{3}\sqrt{(-y')^{3/2}}\right\}\right) \end{aligned} \tag{4.9}$$

(note the prefactor in front of the exponentials, which results from the fluctuations around the saddle points). If y' is sufficiently far away from the critical line $y' = 0$, one can safely disregard the second term in comparison with the first one, and F is of the form $\exp S$. For y' closer to zero, the two saddle points move closer together and the q'-integration can no longer be evaluated by the saddle point approximation, but can be expressed in terms of Bessel functions [13]. At $y' = 0$

$$F \approx \exp 2\xi'^2 = \exp e^{\xi}, \tag{4.10}$$

in agreement with (4.5). The two saddle points in (4.7) correspond to the two trajectories which pass through each point below the ξ'-axis: if we denote the exponents in (4.9) by S_+ and S_-, resp., the equations of motion for ξ' and y' are $\dot{\xi}' = S_{\pm\xi'}, \dot{y}' = S_{\pm y'}$ with the solutions:

$$\begin{aligned} \xi'(\tau) &= \xi'_0 \exp 2\sqrt{2}\tau \approx \xi'_0(1 + 2\sqrt{2}\tau) \\ y'(\tau) &= -\frac{\tau^2}{4}. \end{aligned} \tag{4.11}$$

For small τ these solutions describe parabolas tangent (from below) to the critical line $y \equiv 0$. A similar analysis can also be carried out above the critical line, but this will not be discussed here further. We only emphasize that trajectories never cross the critical line from one side to the other. Finally, we have to return to our old variables ξ and y: the shape of the classical trajectories can be obtained by simple inverting (4.6) and then inserting into (4.11). In the vicinity of the critical line (4.4), the trajectories are straight lines, tangent (from below) to the critical line, in full (qualitative) agreement with the pattern of Fig. 4b. The change of variables in (4.7) is slightly more complicated: the second part in the exponent

$$\tilde{S}'(p,q) = -\frac{1}{4\sqrt{2}} p'^2 - \tfrac{1}{3} q'^3$$

has to be viewed as the Legendre transform of a function $S'(\xi', y')$; in this function we express the primed variables in terms of the unprimed ones and thus obtain $S(\xi, y)$. Now we perform a Legendre transformation with respect to ξ and y and arrive at the new function $\tilde{S}(p,q)$. Apart from a Jacobian (which we ignore since we are only interested in the exponent) the transformed version of (4.7) is of exactly the same form, but with $\tilde{S}(p,q)$ rather than $\tilde{S}'(p',q')$ and unprimed quantities everywhere. The expressions in (4.8), (4.9) remain valid, after the primed variables have been expressed in terms of the unprimed ones.

The main result of this short argument is the following. The simple ansatz $F = \exp S$ has to be used with great care (even if (4.2) is fulfilled). First, near the critical line F is really a sum of two exponentials rather than a single one; moving closer to the line, the two saddle points approach each other and eventually coalesce. Further away from the line, one of the two exponentials becomes negligible compared to the other. The integral representation in (4.7) appears to be the simplest form wich correctly reproduces these features (note, however, that we have been very cavalier about non-exponential factors under the integral. In order to make (4.7) a solution of the nonlinear wave equation, such factors have to be included). Secondly, even away from the critical line, where the ansatz $F = \exp S$ can be justified, there is still an additional prefactor resulting from the fluctuations around the saddle point. When S is very large, its contribution may become negligible, but for realistic values of ξ and y this seems not to be the case (see below). Finally, any semi-classical analysis requires ξ and/or y to be large. Again, for realistic values this may not always be true. In such a case, one has to compute corrections to the leading contributions, which again emphasizes the importance of taking into account the fluctuations. Unfortunately, all this is not merely of academic interest; in particular it seems, as if the critical line is within reach of HERA energies, and the correct treatment of this region, therefore, is a matter of extreme importance.

From a pragmatic point of view, it is clearly very attractive to use the semi-classical approximation scheme in terms of trajectories as a basis for practical computations. The initial conditions along the y-axis (or along some other curve in the (y, ξ) plane) would determine the starting values for the evolution equations, and the whole computation would be reduced to solving ordinary differential equations (what we have said above speaks by no means against such a computational program, it only emphasizes the necessity of doing it carefully). The fact that the "empty" region in Fig. 4b cannot be reached by trajectories that start in the lower region then offers the following attractive possibility. In order to determine the value of the structure function somewhere in the lower part of the (y, ξ)-plane, one needs to know the y-distribution at ξ_0 only inside a finite y-interval, and not for those values of very large y where we would be deep inside the Regge-region. In this sense the GLR equations seem to be self-consistent with respect to the use of perturbative QCD.

Moreover, the boundary line is precisely the line where the GLR-equation ceases to be valid [4]. Beyond this line, fan-diagrams which are the basis for the GLR equations, are not enough and more contributions are expected to become important. For a given initial distribution, the boundary line thus determines the region of applicability. On the other hand, the solution of the GLR equation is smooth across the boundary line. Thus it may very well be that the GLR equation remains qualitatively correct even above this line. This assumption is supported by the fact that the equation leads to saturation at large values of y which is consistent with theoretical expectations. We can also determine the region of validity of the linear evolution. It is the region of all those points which can be reached by a classical trajectory (coming from the left) that has never touched or come close to the boundary line. It lies, approximately, below the tangent to the boundary line at $\xi = \xi_0$. Thus the GLR-equation divides the (y, ξ)-plane into three different regions (including the nonperturbative region where it is no longer valid) [4]. This is quite in contrast to the usual framework if linear evolution [1–3] which formally is valid at all x and Q^2 and does not tell where it becomes inapplicable.

It is now interesting to indicate the transition region in the plots of F versus y at fixed ξ: they are marked with two arrows, respectively, in Fig. 2a and b. At low ξ they almost coincide with the points where the results of nonlinear equation start to deviate from the linear case. This is not surprising since the evolution has hardly taken place. For larger values of Q^2 the critical value in y moves faster towards larger y than that values where linear and nonlinear curves depart from each other. In other words, the "window" where one could see the effects of the nonlinear evolution widens when Q^2 increases.

At the end of this discussion of the use of the semi-classical approximation we return to the feasability of using the trajectories as a basis for doing numerical calculations. First let us try to make our argument concerning the importance of fluctuations more quantitative. As an example, consider (2.6) with $C = 0$ and with the simplest boundary conditions, namely $F = 1$ on both the ξ axis and along the y-axis at $\xi = \xi_0$. Then the solution is known to be $I_0(\sqrt{2y(\xi - \xi_0)})$ where I_0 denotes the

modified Bessel Function.

$$I_0(z) \to \frac{e^z}{\sqrt{2\pi z}}; \quad z = \sqrt{2y(\xi - \xi_0)}. \tag{4.12}$$

An integral representation of this solution is [14]:

$$F(y,\xi) = \int \frac{d\omega}{2\pi i \omega} e^{\omega y + k(\omega)\xi} \tag{4.13}$$

where $k(\omega) = \frac{1}{2\omega}$, and the integration goes along the imaginary axis. When applying the "naive" semi-cassical approximation $F = \exp S$ to this case, one finds the exponential term in (4.12), but not the denominator. The latter one is just the fluctuation factor which we have discussed above. As a numerical example, at $y = 33$ (or $x = 10^{-5}$) and $Q^2 = 10\,\mathrm{GeV}^2$ the exponent is 3.5, whereas the logarithm of the denominator is still 1.6. For $Q^2 = 10^5\,\mathrm{GeV}^2$ the corresponding numbers are 8.9 and 2.0 (we take the logarithm since this appears to be more natural within the semi-classical approximation). This shows that the "naive" semi-classical approximation may be rather inaccurate, even at not so small values of ξ and y.

Finally let us comment on the very recent calculations of Collins and Kwiecinski [6]. They have in fact used the method of trajectories in order to calculate a numerical solution to (2.5) and to determine at what values of ξ, y the nonlinear terms in the GLR equations become important. As input they use a distribution in ξ along the line $y = y_0$ which has been constructed in such a way that, in the absence of the nonlinear term in the evolution equation, it would agree with one of the distributions of Martin, Roberts, and Stirling [15]. Here they choose that distribution which for small x goes as $x^{-3/2}$. As a result, they present the x-distribution at $Q^2 = 4\,\mathrm{GeV}^2$. Because of their different choice of initial condition, we cannot compare directly their results with ours. Qualitatively, the results are consistent with ours, in that they also predict the nonlinear effects to be visible at rather low y-values. Based on the discussion given above, however, we feel that the method that they have used may not be very accurate in the region where they have presented results. It would also be interesting to see, in their calculation, where the critical line is located.

Our conclusion to this part of our discussion is that the ansatz $F = \exp(S)$, for many cases of practical interest, is not good enough, and we have to use a refined version of the semi-classical approximation. The representations (4.7) and (4.13) are first steps in this direction, but before reliable numerical calculations can be done more theoretical work needs to be done. Work along this line is in progress. In the next section we will see that even the approximation (2.5) of the GLR equation is too crude and one has to use, at least, more accurate expressions for the ladders inside the fan diagrams.

5 An improved evolution equation

We now discuss and relax some of the approximations that have been made in deriving (2.5). Let us first consider the linear term describing the standard evolution [1–3]. The latter is given by

$$\begin{aligned}
\frac{\partial G(x,Q^2)}{\partial \ln(Q^2/\Lambda^2)} &= \frac{\alpha_s(Q^2)}{2\pi} \int_x^1 \frac{dz}{z} \\
&\quad \cdot \{P_{gg}(x/z) G(z,Q^2) + P_{gq}(x/z)\Sigma(z,Q^2)\} \\
\frac{\partial \Sigma(x,Q^2)}{\partial \ln(Q^2/\Lambda^2)} &= \frac{\alpha_s(Q^2)}{2\pi} \int_x^1 \frac{dz}{z} \\
&\quad \cdot \{P_{qg}(x/z) G(z,Q^2) + P_{qq}(x/z)\Sigma(z,Q^2)\} \\
\frac{\partial \Delta_f(x,Q^2)}{\partial \ln(Q^2/\Lambda^2)} &= \frac{\alpha_s(Q^2)}{2\pi} \int_x^1 \frac{dz}{z} P_{qq}(x/z)\Delta_f(z,Q^2),
\end{aligned} \tag{5.1}$$

where $\Sigma(x,Q^2) = \Sigma_f[q_f(x,Q^2) + \bar{q}_f(x,Q^2)]$ and $\Delta_f(x,Q^2) = \Sigma_f[q_f(x,Q^2) - \bar{q}_f(x,Q^2)]$. In the limit of small-$x$ the fermionic contributions are small compared to the gluonic ones [16], and the gluon-to-gluon splitting kernel can be approximated by its $x \to 0$ limit:

$$\begin{aligned}
xP_{gg}(x) &= x2N\left[\frac{x}{(1-x)_+} + \frac{1-x}{x} + x(1-x)\right] + \delta(1-x)\frac{\beta_0}{2} \\
&\to 2N.
\end{aligned} \tag{5.2}$$

Changing variables from x and Q^2 to y and ξ, respectively, and setting $F(y,\xi) = xG(x,Q^2)$, (5.1) yields (2.5) (with $C = 0$). The approximation used in (2.5) therefore amounts to approximating the single gluon ladders by their leading contributions both in $1/x$ and in Q^2, i.e. only terms of the form $(\alpha_s(Q^2)\ln(1/x)\ln(Q^2))^n$ are kept. This is why (2.5) (with $C = 0$) is referred to as double-leading-log approximation (DLA). In order to see how serious this approximation is numerically, we compare in Fig. 5 the results of the full standard evolution (5.1) with its DLA limit, i.e. with (2.5) with $C = 0$. We use the parametrization fit S by Morfin and Tung (MT) [17] as input densities at $Q_0^2 = 4\,\mathrm{GeV}^2$ with $\Lambda = 0.212\,\mathrm{GeV}$. As expected, the DLA is not a good approximation at large x. But it differs substantially from the full standard evolution also at small x. In Fig. 5 we also show the result of (2.5), i.e. the DLA including the leading fan contributions. One observes that the deviation of the DLA from the full linear evolution is, in fact, larger than the effect of the

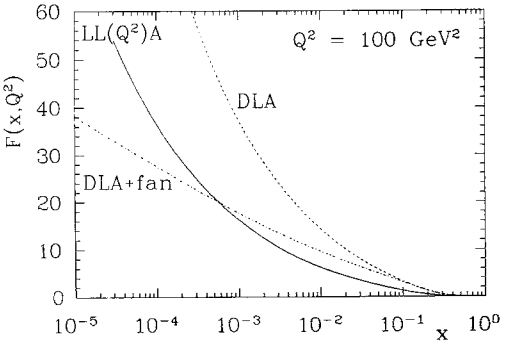

Fig. 5. A comparison between the full standard evolution (5.1, full curve) and its DLA limit ((2.5) with $C = 0$, dashed curve). The dashed-dotted line shows F in the "DLA + fan" approximation, i.e. in the DLA limit with the nonlinear term included

nonlinear term. Thus (2.5) cannot be used to predict the effect of the nonlinear contributions.

An obvious improvement is the inclusion of the full linear evolution Eqs. (5.1) for each ladder inside the fan diagrams. However, since fermionic contributions to the triple ladder vertices of fan diagrams have not been calculated yet, we should, in order to be consistent, neglect the fermionic contributions also inside the ladders. We have checked that in the linear case for $x<0.1$ the inclusion of the fermionic degrees of freedom changes the gluon density by less than a few percent only. Since the effect of the nonlinear term does not set in above $x=0.1$ this is certainly a sufficient approximation. This gives us the following improved evolution equation for the gluon:

$$\frac{\partial F(y,\xi)}{\partial \xi} = \frac{1}{2}\int_0^y dy' \left\{ \frac{z^2 G(y',\xi) - z G(y,\xi)}{1-z} + G(y',\xi)[-z+z^2(1-z)] + G(y',\xi)[1-2Ce^{(-e^{\xi}-\xi)}G(y',\xi)] \right\} + G(y,\xi)\left[\frac{4N}{\beta_0}\ln(1-x)+1\right]. \tag{5.3}$$

Here we defined $z=x/x'=\exp[-(y-y')\beta_0/(8N)]$. Equation (5.3) is our "improvement" of (2.7).

Before we present the solution of this equation we have to discuss the nonperturbative input quantities. As already mentioned in connection with (2.5) the result depends on the input distribution. To explore this kind of dependence we therefore solve (5.3) for two different input distribution: (i) $xG(x,Q_0^2)=(2.62+9.17x)(1-x)^{5.9}$, taken from EHLQ [18] set 1, and (ii) the MT-parametrization $xG(x,Q_0^2)=e^{1.88}x^{-0.33}(1-x)^{7.52}\ln^{-1.34}(1+1/x)$. The EHLQ parametrization represents a density which approaches a constant at small x. In the contrast to this, the Morfin–Tung parametrization is much steeper. Both input distributions are shown in Fig. 6. The other input quantity is the constant C in (5.3). As explained in Sect. 2, C contains a factor describing the relative strength of the two-gluon function relative to the single-gluon distribution function. To test the sensitivity to this parameter we vary C by a factor 2–10 from our canonical value (2.3). Eventually, C has to be fitted together with the input gluon distribution to the data.

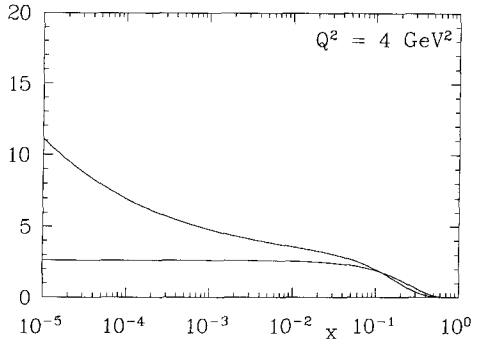

Fig. 6. The input distributions $xG(x,Q_0^2)$ of Morfin–Tung [17] and Eichten et al. [18]

The results of our calculation are given in Fig. 7b–d. They show the gluon density as a function of x for various values of Q^2. The solid curves are the result of the linear evolution, while the dashed lines are the results of the nonlinear evolution with C as given in (2.3). Finally, the dotted lines are obtained by lowering C by a factor of 10. In each case, the upper (lower) curves originate from the MT (EHLQ) input distribution.

Let us list a few observations:

(1) the linear evolution gives rise to a steep increase at small-x even for the flat EHLQ input density. In contrast, the nonlinear evolution flattens the curves.

(2) In the case of the linear evolution, the large difference between the two input densities persists up to high Q^2-values. For the nonlinear case the difference between the two distributions becomes smaller at higher Q^2.

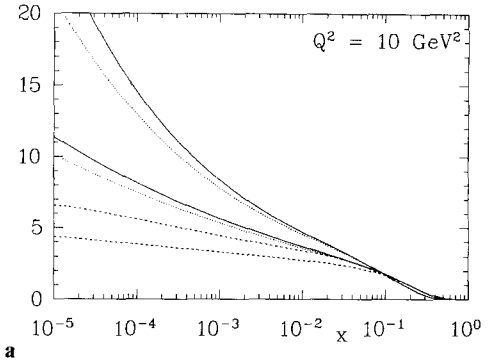

a

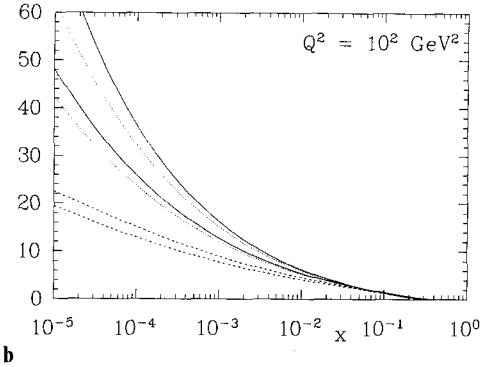

b

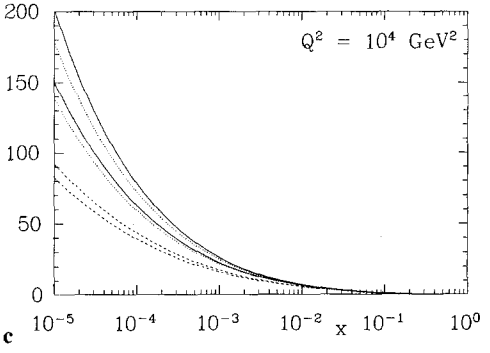

c

Fig. 7 a–c. x-distributions of F for different values of Q^2: **a** $Q^2=10$ GeV^2, **b** $Q^2=10^2$ GeV^2, and **c** $Q^2=10^4$ GeV^2. The full lines belong to the linear equation ($C=0$), the dashed (dotted) ones to the nonlinear case with C of (2.3) ($C\to C/10$). Upper (lower) curves stem from the MT (EHLQ) input distribution

(3) At $Q^2 = 10\,\mathrm{GeV}^2$ the deviation between the standard and the improved evolution solutions starts to set in at $x \sim 0.05$. At $x = 10^{-4}$ the difference is about a factor 2.5. Though the linear solution based on the EHLQ input density is about 30% smaller than the corresponding one obtained from the MT input density, the effect of the nonlinear term is larger. Thus it might be visible at HERA. It should, however, be kept in mind that we are discussing here the gluon structure function. For the structure function F_2 the effect will presumably be less pronounced [19].

(4) At larger Q^2 the onset of the nonlinear flattening is shifted towards smaller values of x.

In Fig. 8 we show the lines in the (x, Q^2) plane where the deviation between the standard and the improved evolution is 10%, 20% and 50%, respectively. Though these lines are obtained from the EHLQ input density, the result for the MT input parametrization is rather similar. Clearly, these lines makes sense only for $Q^2 > 10\,\mathrm{GeV}^2$, since at Q_0^2 both the linear and the nonlinear case were forced to start from the same input density. We observe that the line where the deviation is 20% is approximately at constant $x, x \sim 10^{-2}$. Thus the effect of the nonlinear term might also be observable at higher Q^2, like in the low mass dimuon events in the very forward direction at CDF. Based upon our model calculations of the previous section, we expect that, if at lower Q^2 HERA can really see deviations from the standard linear evolution, then HERA will also reach the nonperturbative region where the parton picture breaks down and the GLR equation cannot be applied: when discussing the arrows in Fig. 2a and b, we noted that at low Q^2 the transition region is very "thin", and only for larger Q^2 it widens. In the same plot we also show the critical curve of [20]:

$$Q_c^2(x) = Q_0^2 + \Lambda^2 \exp\left(3.56\sqrt{\ln\frac{1}{3x}}\right) \tag{5.4}$$

with

$$\Lambda = 52\,\mathrm{MeV}, \quad Q_0^2 = 2\,\mathrm{GeV}^2. \tag{5.5}$$

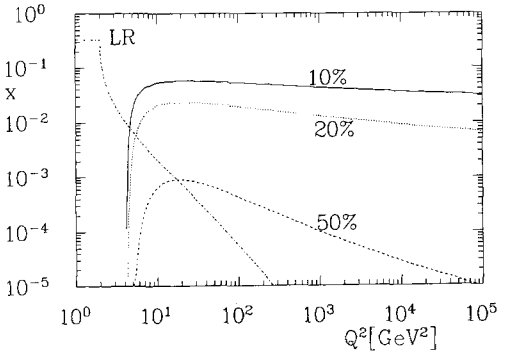

Fig. 8. Comparison of the linear and the nonlinear evolution equations: the full (dotted, dashed) lines indicate where the result of the linear equation differs from the nonlinear one by 10% (20%, 50%). The line marked by "LR" corresponds to (5.4) and denotes the critical line of Levin and Ryskin

If this line is accepted, it confirms the expectation raised above: at $Q^2 = 10\,\mathrm{GeV}^2$ HERA will even reach the nonperturbative region where, strictly speaking, the GLR equation should not be used. We finally mention that we also have tried to produce, proceeding in the same way as for our DLA study, a plot of classical trajectories, analogous to Fig. 4b. The resulting trajectories do not intersect (as they did in Fig. 4b) and, hence, do not produce the boundary line. This indicates that our starting values for ξ and y may have been too close to the critical line, and the naive ansatz $F = e^S$ was not accurate enough.

6 Discussion

In this paper we have performed a numerical study of solutions of the nonlinear Gribov–Levin–Ryskin equation. In the first part we have investigated a simplified version ("DLA + fan" approximation): it allowed us to examine the numerical solution in terms of the semi-classical approximation which, at the moment, is the only available tool for obtaining an analytic solution. In the second part we have tried to define a realistic version of the GLR equation and then solved this equation numerically.

As to the analytic part of our paper, our results are consistent with the findings of [4]. In the (y, ξ)-plane there exists a certain critical line whose exact position depends upon the boundary conditions at, for example, some low Q_0^2. This line separates the region of finite or moderately small x where perturbative QCD is applicable from the nonperturbative Regge limit. The nature of this line as well as the behaviour of the structure function in its vicinity can be analysed in the semi-classical approximation, and we have given a first qualitative discussion. However, this discussion has made clear that for a quantitative analysis the semi-classical approximation has to be used very carefully, i.e. in a more sophisticated version than exploited so far. We believe that more theoretical work will be needed, before a reliable numerical calculation can be done within this approximation.

At the first time a complete numerical solution of the GLR-equation was given. For the simplified version, the "DLA + fan" approximation, we show the behaviour of the solution over a very large range in y and ξ, in particular we demonstrate that at very small x the structure function reaches a plateau: this is consistent with the idea of "saturation". In a more realistic version of the GLR equation, we investigate the dependence on both the initial distribution and the strength of the first fan diagram relative to the standard QCD ladder. The steeper (in y) the initial distribution, the earlier the nonlinear effects will be visible. In particular we find evidence that already at $x = 10^{-2}, Q^2 = 10\,\mathrm{GeV}^2$, deviations from the standard linear evolution may become visible. The numerical solutions depend, as in the case of the linear equations [1–3], on the choice of the input distributions, the QCD-scale Λ and further on the coupling strength C of the fan diagrams. In an analysis of deep inelastic scattering data at low x these parameters will have to be determined consistently.

Note added

After completion of this work we learned that Kwiecinski [21] has obtained a numerical solution of an equation similar (but not identical) to (3) of Sect. 5. In contrast to us he includes the nonlinear term in (5.3) in Sect. 5 only for large $y, y > y_0$, i.e. he replaces the $\int_0^y dy' G^2(y', \xi)$ contribution by $\theta(y-y_0) \int_{y_0}^y dy' G^2(y', \xi)$. As a result of this, the equation agrees no longer with one of the GLR equations. Furthermore he chooses a different input density at $Q^2 = Q_0^2$ as well as different values for Q_0, Λ, and C. Though the absolute normalizations of the gluon densities are different, the relative reduction factors due to the nonlinear term are similar. For example, at $Q^2 = 10\,\mathrm{GeV}^2$ and $x = 10^{-4}$ his difference between the standard evolution and the improved one is about a factor 3.5 whereas in our calculation it is about a factor 2.5. This confirms our conclusion that HERA might already enter a region where deviations from the standard evolution become important.

Acknowledgements. We would like to thank both DESY (JB1) and the Institut für Hochenergiephysik, Zeuthen (JBa and GS) for their hospitality during some visits which have promoted the present work.

References

1. V.N. Gribov, L.N. Lipatov: Sov. J. Nucl. Phys. 15 (1972) 438 and 675
2. G. Altarelli, G. Parisi: Nucl. Phys. 126 (1977) 297
3. Yu. L. Dokshitser: Sov. Phys. JETP 46 (1977) 641
4. L.V. Gribov, E.M. Levin, M.G. Ryskin: Phys. Rep. 100 (1982) 1
5. A.H. Mueller: to appear in the Proceedings of the Small-x Workshop, held at DESY, May 1990 (to be published in Nucl. Phys., ed. A. Ali and J. Bartels)
6. J. Collins, J. Kwiecinski: Nucl. Phys. B335 (1990) 89
7. L.N. Lipatov: Sov. Phys. JETP 63 (1986) 904 and references therein
8. A.H. Mueller, J. Qiu: Nucl. Phys. B268 (1986) 427
9. E. Kamke: Differentialgleichungen, Vol. 2, 5th edition. Leipzig: Geest & Portig 1965
10. A.H. Mueller: Nucl. Phys. B307 (1988) 34; Nucl. Phys. B317 (1989) 573; preprint Columbia Univ. CU-TP-441
11. V.I. Arnold: Mathematical Methods of Classical Mechanics, Appendix 12 and references therein. Berlin, Heidelberg, New York, Tokyo: Springer 1978; in particular: V.I. Arnold: Funct. Anal. Appl. 6 (1972) 254–272
12. M.V. Berry: Semi-classical Mechanics of Regular and Irregular Motion: in Les Houches 1981. G. Iooss, R.H.G. Hellemann, R. Stora (eds.). Amsterdam: North Holland 1983
13. G.N. Watson: A Treatise on the Theory of Bessel Functions, 2nd edition. Cambridge: Cambridge University Press 1958
14. A discussion with M.G. Ryskin on this representation of gratefully acknowledged
15. A.D. Martin, R.G. Roberts, W.J. Stirling: Phys. Rev. D37 (1988) 1161; Mod. Phys. Lett. A4 (1989) 1135
16. J. Blümlein, G. Ingelman, M. Klein, R. Rückl: Z. Phys. C – Particles and Fields 45 (1990) 501
17. J. Morfin, Wu-Ki Tung: preprint Fermilab-Pub 90/74 (1990)
18. E. Eichten et al.: Rev. Mod. Phys. 56 (1984) 579 and Erratum 58 (1986) 1065
19. E.M. Levin, M.G. Ryskin: Frascati Preprint April 1990
20. M.G. Ryskin: Sov. J. Nucl. Phys. 47 (1988) 230
21. J. Kwiecinski: Shadowing effects in parton distributions for small values of x, Durham preprint DTP 90/42 (1990) and to appear in the Proceedings of the Small-x Workshop, held at DESY, May 1990 (to be published in Nucl. Physics, eds. A. Ali and J. Bartels)